AD_____

Award Number: DAMD17-03-1-0666

TITLE: Biological and Genetic Analysis of a New Model for Breast Premalignancy

PRINCIPAL INVESTIGATOR: Carol L. MacLeod, Ph.D.

CONTRACTING ORGANIZATION: University of California, San Diego
La Jolla, California 92093-0934

REPORT DATE: September 2004

TYPE OF REPORT: Final

PREPARED FOR: U.S. Army Medical Research and Materiel Command
Fort Detrick, Maryland 21702-5012

DISTRIBUTION STATEMENT: Approved for Public Release;
Distribution Unlimited

The views, opinions and/or findings contained in this report are those of the author(s) and should not be construed as an official Department of the Army position, policy or decision unless so designated by other documentation.

REPORT DOCUMENTATION PAGE

Form Approved
OMB No. 074-0188

1. AGENCY USE ONLY (Leave blank)	2. REPORT DATE	3. REPORT TYPE AND DATES COVERED
	September 2004	Final (15 Aug 2003 - 14 Aug 2004)

4. TITLE AND SUBTITLE
Biological and Genetic Analysis of a New Model for Breast Premalignancy

5. FUNDING NUMBERS
DAMD17-03-1-0666

6. AUTHOR(S)
Carol L. MacLeod, Ph.D.

7. PERFORMING ORGANIZATION NAME(S) AND ADDRESS(ES)
University of California, San Diego
La Jolla, California 92093-0934

E-Mail: cmacleod@ucsd.edu

8. PERFORMING ORGANIZATION REPORT NUMBER

9. SPONSORING / MONITORING AGENCY NAME(S) AND ADDRESS(ES)
U.S. Army Medical Research and Materiel Command
Fort Detrick, Maryland 21702-5012

10. SPONSORING / MONITORING AGENCY REPORT NUMBER

11. SUPPLEMENTARY NOTES

12a. DISTRIBUTION / AVAILABILITY STATEMENT
Approved for Public Release; Distribution Unlimited

12b. DISTRIBUTION CODE

13. Abstract *(Maximum 200 Words)* *(abstract should contain no proprietary or confidential information)*

The goal of this project was to gain further understanding of premalignant hyperplasia and its role in progression to breast cancer. Most human and mouse model breast cancer research has focused on tumors and metastsis, whereas the biology of premalignant lesions has not been thoroughly studied. We established a new mouse model of premalignant hyperplasia using six serially transplantable, stable, hyperplastic outgrowth cell lines to analyze neoplastic lesions within the intact microenvironment of the mammary gland. These cell lines were ideally suited to DNA microarray to identify changes in gene expression between premalignant cells growing in the mammary gland and tumors that arise from these tissues. Our studies have defined genes differentially expressed in the transition from normal to premalignant mammary disease as well as from premalignant to malignant mammary cancer. The genes related to the malignant transition in our system have also been identified as potential regulators of human breast cancer. The lines developed in this study can be utilized to develop chemoprevention and therapeutic protocols for breast cancer in the future.

14. SUBJECT TERMS
premalignancy, breast cancer, hyperplastic outgrowth lines

15. NUMBER OF PAGES
21

16. PRICE CODE

17. SECURITY CLASSIFICATION OF REPORT	18. SECURITY CLASSIFICATION OF THIS PAGE	19. SECURITY CLASSIFICATION OF ABSTRACT	20. LIMITATION OF ABSTRACT
Unclassified	Unclassified	Unclassified	Unlimited

Table of Contents

Introduction:

The epithelial breast cells responsible for milk production are the major culprits in breast cancer. The excessive and invasive growth of these cells leads to the development of cancer. There are no screening methods available to distinguish benign from premalignant lesions. Premalignant breast lesions predispose women to a higher risk of breast cancer. Our group recently developed a novel approach to understanding the early events in breast disease that precede breast cancer. Our research resulted in the development of a unique new mouse model that has potential benefit to women at risk for breast cancer. Our model is the first available to systematically study premalignancy in breast cancer. Since the genetics of mouse and human breast tumors are very similar, there are three needs that this model has the potential to meet; it can be used to evaluate breast cancer prevention strategies in preclinical trials; it offers a method to test promising therapeutic strategies; it provides reliable and reproducible material that will be used to identify signature genetic changes in expression required for cells to become metastatic tumors and to identify biomarkers, analogous to PSA for prostate cancer that would serve as screening and predictive tools for breast cancer.

Body:

The following personnel were partially funded on this project ; Jeanne E. Maglione; Xianshu Cui; Sarah Davie; Melinda Richards; Steve Shenouda; Petra Paulus

Statement of Work:

Identifying the genetic profiles of normal mammary epithelial cells, premalignant cell and tumors by microarray analysis before and after transformation to malignancy.

Task 1: Prepare tissue samples by transplantation.

Serial transplantation of the pre-malignant MIN-O tissue bilaterally into the gland-cleared no. 4 mammary fat pads of recipient FVB virgin females (The Jackson Laboratory, Bar Harbor, Maine) was carried out at 5-week intervals. MIN-Os and tumors were collected over four consecutive transplant generations (generations 9 to 12). In addition, intact no. 2 and 3 mammary fat pads from the MIN-O transplant animals were collected and used as non-transgenic virgin mammary fat pads. Prelactating mammary fat pads were collected from the no. 4 mammary fat pads of 16-day pregnant FVB animals. Tumors and MIN-O tissues were identified under a stereomicroscope, and grossly distinct regions were carefully biopsied for serial transplantation or sampling for further analysis.

Since the MIN-O growth is confined to within the host mammary fat pad, the MIN-O grows as a flat sheet into the approximate shape of the fat pad. In contrast, tumors emerge from the central regions of the MIN-Os and grow as raised foci of dense tissue with defined borders. Because of this difference in the growth patterns, tumors can be distinguished grossly from surrounding MIN-O tissue. Dissected samples were frozen immediately in liquid nitrogen and stored at -80°C for future molecular analysis. The remaining fat pad from each tumor/MIN-O site was fixed in 4% formalin and embedded in paraffin, and 4-μm sections were stained with Mayer's hematoxylin and eosin (H&E). The biopsied site on the H&E stained sections of the corresponding mammary fat pad were evaluated histologically to confirm the origin of the frozen sample before any samples were used for the molecular studies.

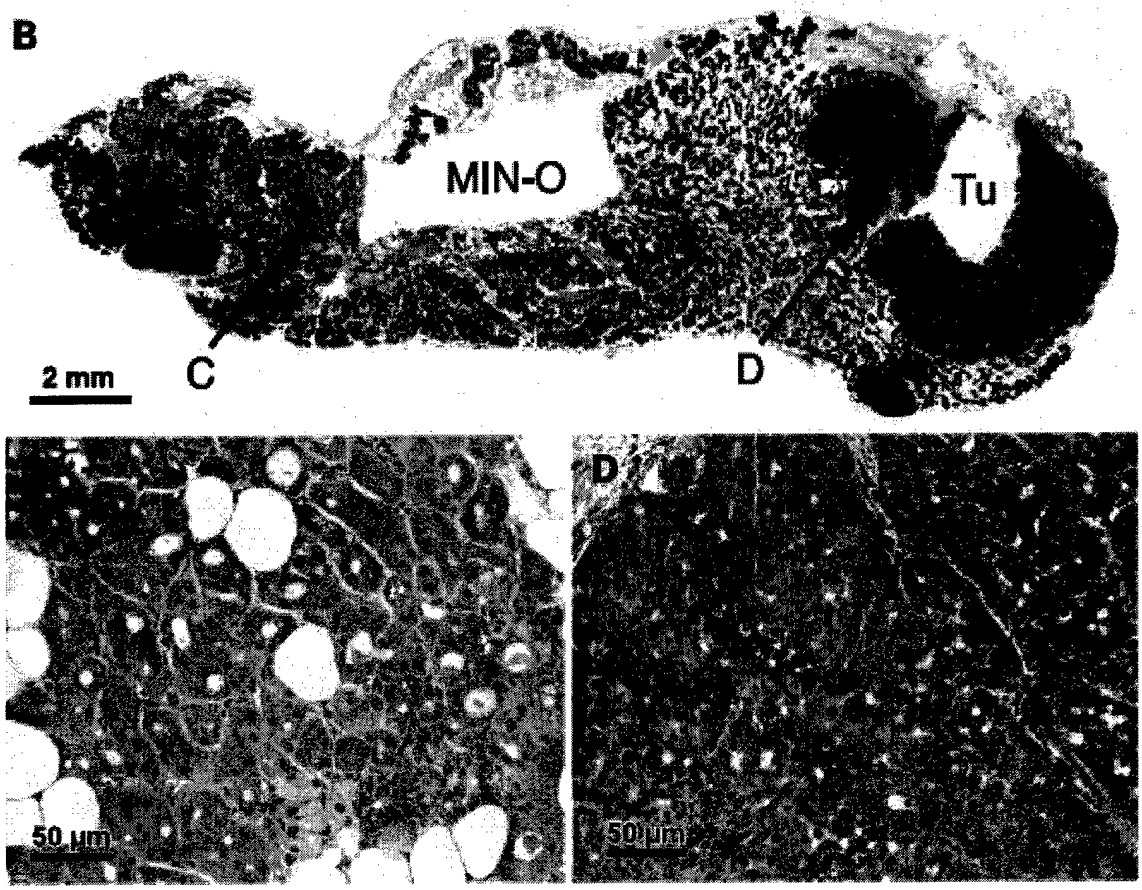

Figure 1. Whole slide image of MIN outgrowth 8w-D and tumor showing the tissue surrounding the MIN outgrowth (MIN-O) and tumor (Tu) biopsies corresponding to 8w-D_5309L samples. This particular outgrowth was composed almost entirely of eosinophilic microacini. C, higher magnification image of the eosinophilic microacini in approximate area (arrow, C) in B. D, higher magnification of the tumor tissue in the approximate area (arrow, D) in B.

Task 2: Identify the genetic profiles of selected Zone 4 premalignant HPO lines and normal mammary cells and their metastatic foci.

Purified total RNA was used for cDNA synthesis, followed by in vitro transcription to incorporate biotin labels and subsequent hybridization to Murine Genome GeneChip U74Av2 (MG_U74Av2, Affymetrix, Santa Clara, CA) according to the manufacturer's protocol. The U74Av2 array represents ~6,000 well-characterized sequences from the mouse Unigene database and an additional ~6,000 less well-characterized sequences from the expressed sequence tag (EST) clusters in the Unigene database.

Data analysis: Processing of individual GeneChip image files was carried out using Affymetrix Microarray Analysis Suite 5.0 (MAS 5.0, Affymetrix). 5,119 probes that were present in all the MIN-O samples were used to calculate the correlation coefficients between different groups of mammary tissue. The image files of the MIN-O, virgin, prelactating, and tumor samples were processed in DNA-Chip Analyzer, version 1.2 (dChip 1.2. The MIN-O and normal (virgin and prelactating) groups were compared to identify probes with at least 2-fold expression difference,

at the lower boundary of the 90% confidence interval, with a pvalue of 0.05 or less.

The same criteria, as well as a less stringent fold change requirement (1.2-fold), were used to compare the MIN-O and tumor image files. On the MAS 5.0 processed image files, pair-wise comparison of each MINO/tumor pair was performed to identify genes with at least 2-fold expression differences in three out of four pairs or 1.2-fold differences in all four pairs. Moreover, using the Data Mining Tool (Affymetrix), the MIN-O expression data was compared to that of the tumor groups to identify probes with at least 1.2-fold expression differences with $p<0.05$. Probes whose detection signal was considered absent in all samples by the MAS 5.0 analysis were removed from the data set, and the remaining probe set data was log transformed and subjected to the Significance Analysis of Microarrays (SAM) to select probes with differential expression of 1.2-fold. The final list of genes was generated from the significant differences from dChip 1.2 (1.2-fold, $p<0.05$), using confirmation with at least one additional methodology (MAS, DMT and SAM) (Supplimental data table 2). Hierarchical clustering analysis was carried out in dChip 1.2 using probes that showed significant variation across the samples, as defined by having a coefficient of variation (standard deviation/mean) greater than 0.3 and being present in at least 50% of samples; a second cluster was developed using the 33 probes that were consistently differentially expressed between the MIN-Os and tumors.

Metastatic foci were not examined in this study as the number of lung metastases formed was not sufficient to carry out the microarray analysis.

Table 1. Metastasis data

Line	Lungs Examined	Lungs with Metastases	Incidence
8w-A	16	8	0.50
8w-B	10	0	0
8w-D	15	7	0.47
4w-4	6	0	0
4w-6	5	0	0
4w-11	16	10	0.63

NOTE: Incidence of metastasis in lungs of mice with MIN outgrowth line tumors. Emerging tumors were allowed to grow for 60 days or until they reached the maximum allowable size limit. Whole mounts of lungs were examined. Several metastases from each line were confirmed histologically. Metastases were frequently observed in several of the lines. However, no metastases were observed in mice carrying lines 8w-B, 4w-4, or 4w-6.

Task 3: Identifying new genes previously unsuspected for their participation in the pathway from premalignancy to malignancy.

To identify genes associated with the malignant transition from MIN-O to tumor, we compared the gene expression of the MIN-O and their paired tumors. Because our initial analysis found a

high correlation of the MIN-O and tumor expression profiles from the same mammary fat pad, pair-wise comparisons of the MIN-O and tumor pairs were done to identify differences specific to this transition in each pair. We found 43 genes that were differentially expressed with at least a 2-fold change in three of four MIN-O and tumor pairs. When the same criteria used for the analysis on the premalignant transition were applied to MIN-O/tumor transition, a total of five genes— all of which were down-regulated in tumors—were found (Scd1, Cdo1, Acrp30, Adn, and Car3). This suggests that only a few subtle expression differences are associated with the malignant transition as compared with the premalignant transition. The majority of changes occur between normal and premalignant tissues. (see Table 1, Namba et al., 2004).

Validating the genetic profile results from Tasks 1 –3, determining if they are found in other HPO tumors and metastases

Task 4: Validate the identified changes in gene expression to determine whether the changes detected by microarray are confirmed by independent classical methods of Immunocytochemistry.

Immunohistochemistry (IHC): IHC was performed on 4µm paraffin sections. The following primary antibodies were used with the VECTASTAIN ABC Elite Kit (Vector Laboratories, Burlingame, CA): rabbit anti-estrogen receptor (ER, 1:600, LabVision, Fremont, CA), rabbit anti-PyV-mT (1:400, gift from Dr. G. Walter, UCSD), rabbit anti-Decorin (1:300, R&D systems Inc., Minneapolis, MN), rabbit anti- IGFBP2 (1:400, Santa Cruz Biotechnology, Santa Cruz, CA), rabbit anti-progesterone receptor (PR, 1:500, DAKO, Carpinteria, CA), anti-Ki67 (1:2400, Novocastra Laboratories, Newcastle upon Tyne, UK). Anti-smooth muscle actin (SMA, 1:1000, DAKO) was used in conjunction with the Animal Research Kit (DAKO) according to the manufacturer's instructions.

For two genes, immunohistochemistry was used to verify and localize the protein products of differentially expressed genes. According to the expression analysis, insulin-like growth factor binding protein-2 (Igfbp2) exhibited increased expression in tumors, while it was scarcely expressed in the normal fat pads. In the MINOs, patchy cytoplasmic expression was detected. In the center, away from the proliferative peripheral region, some myoepithelium-like staining was observed. However, this pattern did not overlap with smooth muscle actin (SMA) expression, and thus it is unlikely that these Igfbp2 positive cells are myoepithelial. In the tumors, Igfbp2 was expressed at higher levels in a global cytoplasmic pattern with random patches of very strong positivity within the tumor. Decorin (Dcn) was one of the genes down-regulated at the malignant transition. Dcn is a small proteoglycan of extracellular matrix (ECM) that is known to be dysregulated in human breast carcinoma. The transcript level of Dcn was down-regulated by more than two fold at the MIN-O/tumor transition, while the samples of normal tissue had even higher expression levels than the MIN-Os. Dcn was expressed throughout the stroma of prelactating fat pads. Interestingly, in the prelactating fat pads, the strongest staining of Dcn was found to highlight septa within the stroma.

See Fig. 5 Namba et al. 2004 for results.

Task 5: Final analysis and reports.

Processing of individual GeneChip image files was carried out using Affymetrix MAS 5.0. Probes (n = 5,119) that were present in all the MIN-O samples were used to calculate the correlation coefficients between different groups of mammary tissue. The image files of the MIN-

O, virgin, prelactating, and tumor samples were processed in DNA-Chip Analyzer version 1.2. The MIN-O and normal (virgin and prelactating) groups were compared to identify probes with at least 2-fold expression difference, at the lower boundary of the 90% confidence interval, with P V 0.05. The same criteria, as well as a less stringent fold change requirement (1.2-fold), were used to compare the MIN-O and tumor image files. On the MAS 5.0 processed image files, pair-wise comparison of each MIN-O and tumor pair was done to identify genes with at least 2-fold expression differences in three of four pairs or 1.2-fold differences in all four pairs. Moreover, using the Data Mining Tool (Affymetrix), the MIN-O expression data were compared with that of the tumor groups to identify probes with at least 1.2-fold expression differences with $P < 0.05$. Probes, with detection signal considered absent in all samples by the MAS 5.0 analysis, were removed from the data set, and the remaining probe set data were log transformed and subjected to the Significance Analysis of Microarrays to select probes with differential expression of 1.2-fold. The final list of genes was generated from the significant differences from DNA-Chip Analyzer version 1.2 (1.2-fold, $P < 0.05$) using confirmation with at least one additional methodology (MAS 5.0, Data Mining Tool, and Significance Analysis of Microarrays).4 Hierarchical clustering analysis was carried out in DNAChip Analyzer version 1.2 using probes that showed significant variation across the samples, as defined by having a coefficient of variation (SD/mean) of >0.3 and being present in at least 50% of samples; a second cluster was developed using the 33 probes that were consistently differentially expressed between the MIN-Os and tumors.

In summary, our data support the hypothesis that the molecular changes occur very early in the progression to cancer and prior to the histopathological identification of invasive cancer. The data presented here demonstrate that the transition from premalignancy to invasive carcinoma is associated with relatively few additional changes in gene expression. The genes related to the malignant transition in our GEM derived model have also been identified as potential regulators of human breast cancer. These genes provide evidence for the dysregulation of the mitogenic signaling and the stromalepithelial interaction as key regulators in the transition to invasive carcinoma. We propose that this model closely mimics the development of invasive carcinoma in human breast. Together with other PyV-mT MIN-O lines, the 8W-B line provides an experimental system for understanding the biology of heterogeneous human DCIS lesions. These lines can be utilized to develop chemoprevention and therapeutic protocols for breast cancer in the future.

One manuscript resulting from this project is appended.

Key Research Accomplishments:

1. MIN-O and tumor pairs have very similar gene expression profiles.
2. 132 gene showed large expression differences between MIN-Os and virgin and prelactating mammary glands.
3. 5 genes were found to be consistently differentially expressed between MIN-Os and tumors
4. The MIN-O model has been proven to provide information important in defining molecular changes from normal to premalignant to malignant cancer.

Reportable Outcomes:

Manuscripts:

Namba R, Maglione JE, Young LJT, Borowsky AD, Cardiff RD, MacLeod CL, and Gregg JP; Molecular characterization of a mouse model for ductal carcinoma in situ (DCIS). Mol Cancer

Res 2004;2(8):453–63)

Abstracts:

Maglione JE , McGoldrick ET, Young LJT, Namba R, Gregg JP, Moghanaki D, Ellies LG, Borowsky AD, Cardiff RD, and **MacLeod CL**. PyV-mT-induced MIN outgrowths: Single origin, divergent evolution, multiple outcomes. International Association for Breast Cancer Research, Sacramento, CA, 2003.

Conclusion:

Our data support the hypothesis that the molecular changes occur very early in the progression to cancer and prior to the histopathological identification of invasive cancer. The data presented here demonstrate that the transition from premalignancy to invasive carcinoma is associated with relatively few additional changes in gene expression. The genes related to the malignant transition in our GEM derived model have also been identified as potential regulators of human breast cancer. These genes provide evidence for the dysregulation of the mitogenic signaling and the stromalepithelial interaction as key regulators in the transition to invasive carcinoma.

"So what"

We propose that this model closely mimics the development of invasive carcinoma in human breast. Together with other PyV-mT MIN-O lines, the 8W-B line provides an experimental system for understanding the biology of heterogeneous human DCIS lesions. These lines can be utilized to develop chemoprevention and therapeutic protocols for breast cancer in the future.

References

1. **Howard, B. A., and Gusterson, B. A.:** Human Breast Development. *J Mammary Gland Biol. Neoplasia,* 5(2): 119-137, 2000.
2. **Maglione, J.; Moghanaki, D.; Young, L. J. T.; Manner, C. K.; Nicholson, B.; Kleeman, J.; Cardiff, R. D.; and MacLeod, C. L.:** Transgenic Polyoma Middle-T Mice Model Premalignant Mammary Disease. *Cancer Research,* 61(22): 8298-305, 2001.
3. **Mallon, E.; Osin, P.; Nasiri, N.; Blain, I.; Howard, B.; and Gusterson, B.:** The basic pathology of human breast cancer. *J Mammary Gland Biol Neoplasia,* 5(2): 139-63, 2000.
4. **Medina, D.:** Preneoplasia in mammary tumorigenesis. *Cancer Treatment and Research,* 83: 37-69, 1996.
5. **Page, D. L.; Jensen, R. A.; and Simpson, J. F.:** Premalignant and malignant disease of the breast: the roles of the pathologist. *Modern Pathology,* 11(2): 120-8, 1998.
6. **Maglione JE, McGoldrick ET, Young LJT, Namba R, Gregg JP, Liu L, Moghanaki D, Ellies LG, Borowsky AD, Cardiff RD, and MacLeod, CL;** PyV-mT-induced MIN

outgrowths: Single origin, divergent evolution, multiple outcomes. (2004), *In Press Molecular Cancer Therepeutics.*

Molecular Characterization of the Transition to Malignancy in a Genetically Engineered Mouse-Based Model of Ductal Carcinoma *In situ*

Ruria Namba,[1] Jeannie E. Maglione,[2] Lawrence J.T. Young,[2] Alexander D. Borowsky,[1,2] Robert D. Cardiff,[1,2] Carol L. MacLeod,[3] and Jeffrey P. Gregg[1]

[1]Department of Pathology and Laboratory Medicine, School of Medicine and [2]Center for Comparative Medicine, University of California-Davis, Sacramento, California and [3]Department of Medicine, School of Medicine, University of California-San Diego Cancer Center, La Jolla, California

Abstract

A transplantable model of human ductal carcinoma *in situ* that progresses to invasive carcinoma was developed from a genetically engineered mouse (GEM). Additional lines were established using early mammary premalignant lesions from transgenic MMTV-PyV-mT mice. These lines were verified to be premalignant and transplanted repeatedly to establish stable and predictable properties. Here, we report the first in-depth molecular analysis of neoplastic progression occurring in one premalignant transplantable GEM-derived line. Oligonucleotide microarrays showed that many genes are differentially expressed between the quiescent and prelactating mammary gland and the premalignant GEM outgrowth. In contrast, a small but consistent group of genes was associated with the transformation from premalignancy to tumor. This suggests that the majority of gene expression changes occur during the premalignant transition from normal to premalignancy, whereas many fewer changes occur during the malignant transition from premalignancy to invasive carcinoma. The premalignant transition is associated with several cell cycle–related genes and the up-regulation of oncogenes is associated with various cancers (*Ccnd11*, *Cdk4*, *Myb*, and *Ect2*). The changes identified in the malignant transition included genes previously associated with human breast cancer progression. Misregulation of the insulin-like growth factor and transforming growth factor-β signaling pathways and the stromal-epithelial interaction were implicated. Our results suggest that this transplantable GEM-based model recapitulates human ductal carcinoma *in situ* at both histologic and molecular levels. With consistent tumor latency and molecular profiles, this model provides an experimental platform that can be used to assess functional genomics and molecular pharmacology and to test promising chemoprevention strategies.

(Mol Cancer Res 2004;2(8):453–63)

Introduction

Studies suggest that development of human breast cancer is a multistep process, starting from a benign stage and progressing through histologically distinct intermediate proliferative stages of hyperplastic epithelium that ultimately results in invasive cancer (1, 2). Ductal carcinoma *in situ* (DCIS) is a preinvasive lesion of the human breast and accounts for up to 20% of newly diagnosed breast cancer cases in the United States, according to National Cancer Institute statistics (http://www.cancer.gov). Although detailed molecular studies of DCIS have been published in recent years (3-5), and DCIS has just begun to be modeled in genetically engineered mice (GEM; refs. 6-8), the stages of hyperplasia that precede DCIS and the mechanism(s) of disease progression are not well understood.

We developed a mouse model of DCIS that recapitulates "premalignant" disease of the mammary gland to probe the molecular biology of DCIS (9). This model is based on the transgenic mouse with mammary-specific expression of the polyomavirus middle T transgene (PyV-mT; refs. 8, 10). The PyV-mT GEM model is attractive, as it recruits and activates a variety of signaling molecules associated with human breast carcinoma, including those that interact with ErbB2. Neu/ErbB2, a receptor tyrosine kinase, is overexpressed in 30% to 40% of human breast cancer and is associated with a poor outcome (11-14). Histologically, the PyV-mT tumors resemble activated ErbB2 tumors in mice and human breast cancer much more closely than do other GEM mammary tumors (15, 16). Moreover, at the transcriptome level, the PyV-mT and neu/ErbB2 GEM mammary tumors are very similar as seen by microarray analysis (17). As in human breast cancer, PyV-mT tumors arise as focal atypical proliferative lesions in the mammary gland that eventually progress to malignant tumors. Moreover, the morphologically distinct stages are histopathologically very similar to various stages of human breast cancer progression (9, 16).

Over the last several years, stable mammary intraepithelial neoplasia (MIN) outgrowth (MIN-O) lines have been developed

Received 5/10/04; revised 6/30/04; accepted 7/12/04.
Grant support: National Cancer Institute grants CA89140-01 (R.D. Cardiff and J.P. Gregg) and 5R01CA81736 (C.L. MacLeod), Department of Defense grant DAMD 17-03-1-0666 (C.L. MacLeod), California Breast Cancer Research Program grants 6KB-0074 (J.P. Gregg) and 9FB-0212 (R. Namba), National Centers for Research Resources grant U42RR14905, and IF Smith Foundation.
The costs of publication of this article were defrayed in part by the payment of page charges. This article must therefore be hereby marked advertisement in accordance with 18 U.S.C. Section 1734 solely to indicate this fact.
Requests for reprints: Jeffrey P. Gregg, Department of Pathology and Laboratory Medicine, School of Medicine, University of California-Davis, 2805 50th Street, Sacramento, CA 95817. Phone: 916-703-0362; Fax: 916-703-0367. E-mail: jpgregg@ucdavis.edu

from early dysplastic foci from the PyV-mT mice (9). Dysplastic foci in the developing PyV-mT GEM mammary gland were macroscopically dissected and transplanted into the gland-cleared mammary fat pads of host FVB females. The dysplastic outgrowths grow to fill the fat pad (see Fig. 1A for description). Individual foci were developed into independent MIN-O lines. Although the MIN lesions, which by definition are premalignant (18), will grow in the orthotopic location in perpetuity, they will not grow subcutaneously. Eventually, malignant tumor foci, which will grow in both orthotopic and s.c. locations, arise within the MIN-O, demonstrating its biological potential. These criteria provide operational definition of "premalignancy" and "malignancy." In addition, the outgrowth can be sampled and transferred to other mammary fat pads, effectively amplifying the original transplant. Each transplant line has a consistent growth rate and tumor latency period (19). Medina et al. have developed similar lines from p53-null GEM in the BALB/c background (20, 21). The ability to develop, propagate, and expand the MIN-O lines in the cleared mammary fat pad of immunocompetent syngeneic mice provides the opportunity for detailed phenotypic (histology, tumor latency, and metastasis rate) and molecular analysis of transitions in neoplastic states.

Here, we report the detailed molecular analysis of neoplastic progression in one of the six transplantable MIN-O lines (8w-B). This line was chosen because of its relatively short tumor latency (11 weeks) and uniform histopathology (19). Sample pairs from individual MIN-Os and their corresponding tumors from the same mammary fat pads were studied over multiple transplant generations. Despite passaging through multiple transplant donors, the histopathology and tumor latency of the MIN-Os remained stable. A large number of genes were found with significant expression differences between the MIN-O and the quiescent or prelactating mammary gland. Many of these

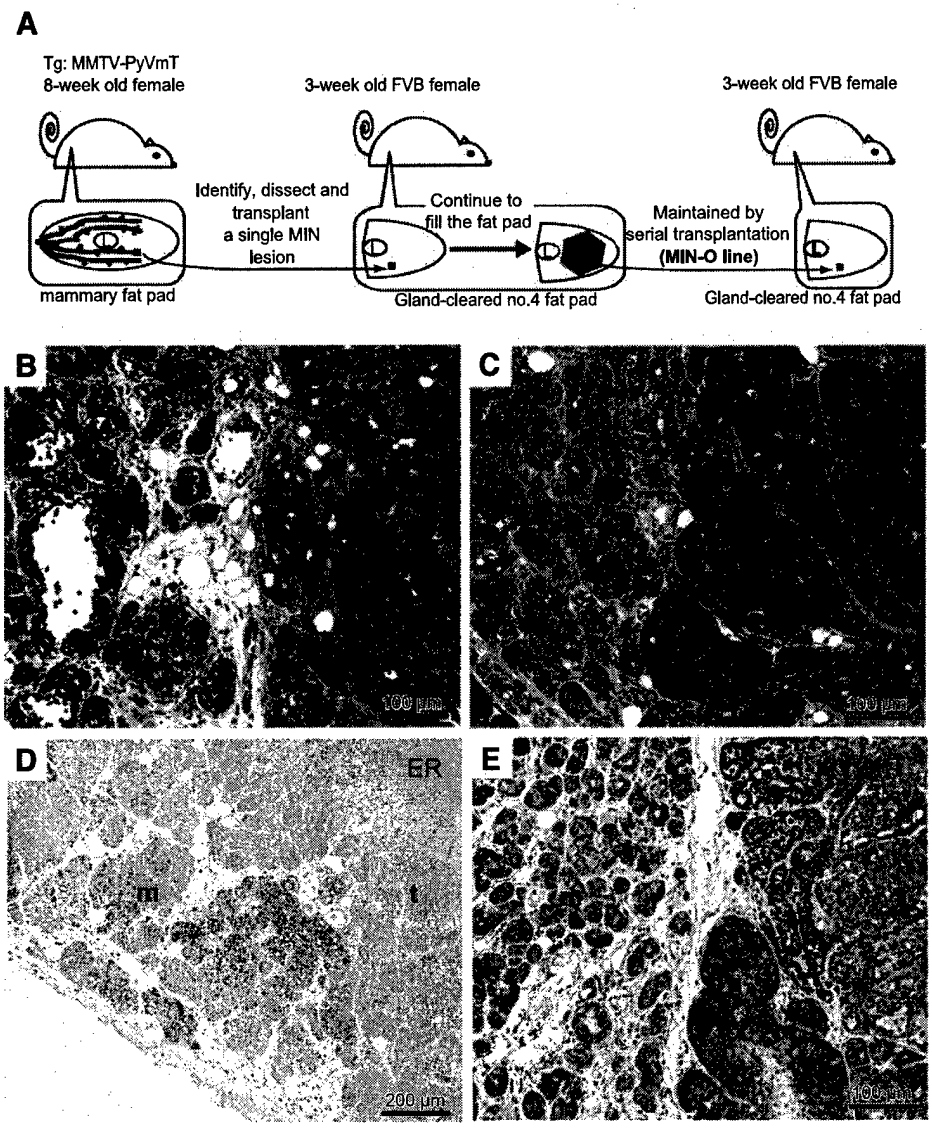

FIGURE 1. Scheme of derivation and maintenance of PyV-mT GEM-derived MIN-O lines (**A**). A small lesion from a MMTV-PyV-mT mammary fat pad was transplanted to a no. 4 mammary fat pad of a 3-week-old FVB female. The host FVB fat pad was gland cleared by removing the area between the nipple and the lymph node (*L*). Morphologic (**B** and **C**) and IHC (**D** and **E**) characterization of MIN-O and tumor. In the mammary fat pads of the 8w-B line, dysplastic cysts (**B**), microacini, and solid nests of cells (**C**) were common patterns observed in MIN-Os (*m*). Tumors (*t*) were typically solid and undifferentiated (**B** and **C**). Patches of estrogen receptor (*ER*)–positive cells were observed in MIN-Os (**D**). IHC staining with anti-PyV-mT (**E**) show fairly uniform PyV-mT expression across the tumor/MIN-O interface. Corresponding H&E staining is shown in **C**.

genes have been associated with human breast cancer. In contrast, only a few differentially expressed genes were associated with the malignant transformation from MIN-O to tumor. This suggests that early lesions already carry changes in most of the "oncogenic" program that are similar to what has been described in human breast cancer (3). In addition, the changes identified in the malignant transition from the MIN-O to tumor included genes previously associated with human breast cancer progression. In summary, these results suggest that this transplantable GEM-based model recapitulates human DCIS and its progression to invasive carcinoma at both histologic and molecular levels.

Results

Mouse Mammary Intraepithelial Outgrowth Line

The morphology and histology of the MIN-Os were characteristics of the line 8w-B as described previously (19). Cells comprising the MIN-Os were organized according to several distinct patterns of differentiation including dysplastic cysts, microacini, and solid nests of cells (Fig. 1B and C). The most abundant structures, dysplastic cysts, were lined by one to eight layers of pleomorphic cells (Fig. 1B). However, despite organization into distinct patterns of differentiation, an organized layer of smooth muscle actin–positive myoepithelium was not observed. Patches of MIN-O cells positive for estrogen receptor were frequently observed (Fig. 1D). In contrast, progesterone receptor was not detected in MIN-Os.

The average tumor latency among the analyzed samples was 11.9 (SE, 4.4) weeks and did not significantly differ from that reported previously for this line (19). Tumors were in the central, more differentiated regions of the outgrowth rather than at the proliferating periphery. Histologically, the tumors were solid, undifferentiated masses of highly pleomorphic cells, and in some areas, more organized groups of cells formed microacini (Fig. 1B and C). These tumor phenotypes are characteristic of this system (9, 16, 19).

Semiquantitative reverse transcription-PCR (RT-PCR) and immunohistochemistry (IHC) were used to examine the levels of PyV-mT transgene expression in both MIN-Os and tumors. The PyV-mT expression at the transcript and protein level was uniform between MIN-Os and tumors (Fig. 1E). There was no obvious correlation of the PyV-mT expression pattern with the proliferation state based on the Ki67 IHC staining (data not shown). These results suggest that progression from premalignancy to invasive carcinoma is, at least in part, driven by secondary molecular changes rather than changes in PyV-mT transgene expression.

Gene Expression Analysis

RNA from the MIN-O and tumor from the same mammary fat pad was used for the gene expression analysis on the Murine Genome Array U74Av2 (Affymetrix, Santa Clara, CA). A total of four MIN-O and tumor pairs from the different serial transplant generations were used. In addition, mammary fat pads from nontransgenic virgin and prelactating FVB females were used as "normal" samples. To understand the global gene expression trend of the tissues, we calculated the correlation coefficients (r^2) of the samples using values from 5,119 probes that were identified as present in all four MIN-O samples (Fig. 2A). The expression profiles of the MIN-Os were highly similar over four transplant generations ($r^2 = 0.948-0.979$). In contrast, the correlation coefficients between the profiles of the prelactating and virgin fat pads and those of the outgrowths were much lower ($r^2 = 0.788-0.877$). The molecular similarity of the MIN-Os is further supported by the observation that the MIN-Os maintained their morphologic and histologic characteristics over multiple generations. The expression profiles of the tumors arising from the MIN-Os were also highly similar ($r^2 = 0.947-0.982$). Interestingly, the correlation coefficients of the MIN-Os and their tumors were also very high ($r^2 = 0.941-0.982$). This suggests that the transcriptional profile of the MIN-Os and tumors are extremely similar despite their differences in neoplastic potential.

To better understand the relationships between MIN-Os and tumors, 654 genes with significant variation of expression level across samples were used to hierarchically cluster the samples (Fig. 2B). By using an unbiased set of genes that were selected based on their variation rather than on the differential expression between the groups, the tumor and corresponding MIN-O from the same mammary fat pad grouped together in each pair, indicating that the MIN-O and tumor pairs have very similar gene expression profiles. This is intriguing, as the morphologic and phenotypic differences between the MIN-O and tumor are substantial; yet, there seems to be more similarity between the MIN-O and tumor pair in terms of gene expression than within the MIN-O group or the tumor group.

A

	Prelactating MG	Virgin MG	MINO	Tumor
Prelactating MG	0.97	0.783-0.878	0.817-0.877	0.787-0.866
Virgin MG	0.783-0.878	0.955	0.788-0.823	0.736-0.765
MINO	0.817-0.877	0.788-0.823	0.948-0.979	0.941-0.982
Tumor	0.787-0.866	0.736-0.765	0.941-0.982	0.947-0.982

B

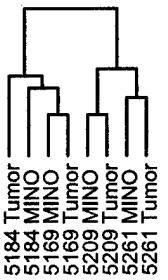

FIGURE 2. Correlation coefficients of tumor, MIN-O, virgin, and prelactating mammary fat pads (**A**). Correlation coefficients were calculated using 5,119 probes that had a "present" detection call in all four MIN-O samples. Hierarchical clustering of MIN-O and tumor samples (**B**). Four pairs of MIN-O and tumor samples were hierarchically clustered using probes with significant variation across the samples. Quantitated value of distance between clusters can be found in Supplemental data 3, available online at http://mcr.aacrjournals.org/.

Expression Differences at the Premalignant Transition

The expression profile of the MIN-Os was very different from that of the normal fat pads based on the correlation coefficients (Fig. 2A). When the MIN-O expression data were compared with the expression data of the virgin and prelactating fat pads, we found 132 genes with large expression differences (Supplemental data 1).[4] Among them, 90 genes had higher expression in the MIN-O. According to the gene ontology analysis, many of these genes are involved in cell proliferation (23 genes; e.g., *Myb*, *Top2a*, *Cks2*, *Ccnb1*, *Ccnb2*, *Ccnd1*, and *Rrm2*), nucleic acid metabolism (21 genes; e.g., *Bub1*, *Stk6*, *Nol5*, *Hspe1*, *Cdc25c*, and *Ran*), and transport (7 genes; e.g., *Kpna2*, *Apod*, *Rasl2-9*, and *Kif20a*). Many of these genes are already known to be associated with cancers (*Ccnd1*, *Cdk4*, *Cdc2a*, *Ccnb1*, *Cdc25c*, *Bub1*, *Stk6*, *Ccnb2*, *Myb*, *Ect2*, and *Top2a*). The genes with higher expression in the normal fat pads are mostly involved in metabolism, including lipid, organic acid, and carbohydrate metabolism (14, 10, and 7 genes, respectively). Because these differences were extrapolated by comparing MIN-Os with both adipose-enriched virgin fat pads and epithelial gland–enriched prelactating fat pads, they are less likely to reflect the contribution from varying cell type composition. Moreover, only a few genes previously classified as adipose specific (*Cd36*, *Fabp4*, *G3pdh1*, *Lpl*, *Pparg*, and *Spp1*) were identified in our list (17, 22).

Expression Differences at the Malignant Transition

To identify genes associated with the malignant transition from MIN-O to tumor, we compared the gene expression of the MIN-O and their paired tumors. Because our initial analysis found a high correlation of the MIN-O and tumor expression profiles from the same mammary fat pad, pair-wise comparisons of the MIN-O and tumor pairs were done to identify differences specific to this transition in each pair. We found 43 genes that were differentially expressed with at least a 2-fold change in three of four MIN-O and tumor pairs. When the same criteria used for the analysis on the premalignant transition were applied to MIN-O/tumor transition, a total of five genes—all of which were down-regulated in tumors—were found (*Scd1*, *Cdo1*, *Acrp30*, *Adn*, and *Car3*). This suggests that only a few subtle expression differences are associated with the malignant transition as compared with the premalignant transition.

To find a more exhaustive number of expression changes associated with the tumor progression, these data sets were subjected to various analytic methods with less stringent criteria (1.2-fold difference), and a set of consistent differences was identified. First, the signal values calculated in the Affymetrix Microarray Analysis Suite 5.0 (MAS 5.0) were subjected to *t* test to identify statistically significant differences. Alternatively, the signal values were log transformed and subjected to Significance Analysis of Microarrays. This method is more sensitive in identifying small changes in gene expression compared with the conventional methods. In addition, the image files were processed and analyzed in DNA-Chip Analyzer version 1.2. The cumulative results from these methods were used to identify a set of consistent expression differences between the MIN-Os and the tumors. As expected from their high correlation coefficient, a few genes were differentially expressed between the two sample types (Table 1 and Supplemental data 2).[4] At the malignant transition, more genes (27 genes; Table 1A) were down-regulated (i.e., lower expression in the tumors compared with the MIN-Os) than were up-regulated (5 genes; Table 1B). Among them, eight genes (*Socs3*, *Igfbp2*, *Chi3l1*, *Lum*, *Dcn*, *Gsn*, *Thrsp*, and *Sncg*) have been reported to be dysregulated in human breast cancer (23-34).

Among the 27 down-regulated genes, many are involved in lipid metabolism and were highly expressed in the virgin fat pad samples. Moreover, a few (*Lpl*, *Adn*, and *Car3*) have been associated with adipose-enriched mouse mammary tissue (17, 22). Thus, we suspected that a subset of these genes may seem down-regulated in tumors because the MIN-Os contain adipose cells in the surrounding stroma, whereas the solid tumors are enriched with epithelial cells. To assess the gene expression differences from the stromal contribution, we used total RNA from two prelactating mammary fat pads for gene expression analysis. Unlike the virgin fat pads, the prelactating mammary fat pad is enriched with proliferating epithelial cells and therefore provides a better control for the proliferative MIN-O tissue. Virgin and prelactating fat pads, MIN-Os, and tumors were hierarchically clustered based on the expression of the identified malignant transition genes (Fig. 3). The 27 genes down-regulated at the malignant transition were clustered into several groups based on their expression pattern in the virgin and prelactating tissues. The first group (*Facl2*, *Thrsp*, *Lpl*, and *Scd1*) was highly expressed in both prelactating and virgin mammary fat pads and was down-regulated in the MIN-Os and more so in the tumors (Table 1Aa and Fig. 3a). We classified these as a group of genes representing the premalignant transition from normal to MIN-O because of the large expression differences between the normal and the MIN-O samples. The second group was associated with very high expression in the adipose-enriched virgin fat pads and therefore represents potential markers for stroma enrichment. Based on the expression in prelactating and MIN-O samples, this second group of genes was subclassified into three classes (Fig. 3b-d). Many were expressed higher in the prelactating fat pads than in the MIN-Os (Table 1Ab and Fig. 3b), whereas a few genes (*Dpt*, *Adn*, *Car3*, *Lum*, and *Dcn*) had similar expression levels in the prelactating and MIN-Os (Table 1Ac and Fig. 3c). Moreover, two genes (*Serping1* and *Hal*) had lower expression in prelactating samples compared with the MIN-Os and tumors (Table 1Ad and Fig. 3d). All the identified genes up-regulated at the malignant transition had a lower expression in the prelactating and virgin mammary fat pads than in the MIN-Os and tumors. This result suggests that the identified malignant transition genes are regulated differently than in the normal proliferating mammary fat pad.

Validation of Expression Differences

Quantitative RT-PCR was used to validate the results of the microarray analysis. We carried out real-time semiquantitative PCR on two of the breast cancer–associated genes (*Thrsp* and

[4] Supplemental data are available online at http://mcr.aacrjournals.org/.

Table 1. Genes Differentially Expressed at the MIN-O/Tumor Transition

Probe ID	Gene	FC*	*P*	Biological Function	Cellular Component
A. Genes down-regulated in tumors at malignant transition					
a.					
94507_at	*Facl2*	2.11	0.045	Fatty acid metabolism	
95020_at	*9130415E20Rik*	1.34	0.025		
160306_at	*Thrsp*	2.45	0.002		Nucleus
95611_at	*Lpl*	4.16	0.003	Lipid metabolism	Extracellular space
94056_at	*Scd1*	2.96	<0.001	Fatty acid biosynthesis	Membrane
94057_at	*Scd1*	2.96	<0.001	Fatty acid biosynthesis	Membrane
b.					
161900_f_at	*Adrb3*	3.91	0.032		
100567_at	*Fabp4*	2.18	0.013	Lipid transport	
97520_s_at	*Nnat*	3.23	0.003	Development	
92718_at	*Isg12*	2.82	0.024		
102366_at	*Retn*	6.37	0.025	Adipocyte hormone	Extracellular space
98924_at	*Art3*	2.67	0.012	Protein amino acid ADP-ribosylation	Extracellular space
99104_at	*Acrp30*	5.45	0.028	Fatty acid β-oxidation	Extracellular space
93750_at	*Gsn*	3.08	0.025	Actin cytoskeleton	Extracellular space
101991_at	*Fmo1*	1.93	0.02	Electron transport	Extracellular space
101539_f_at	*Ces3*	4.66	0.012	Extracellular space	
102373_at	*Enpep*	2.41	0.009	Defense response	Membrane
96346_at	*Cdo1*	4.66	0.023	Taurine metabolism	
104280_at	*Sncg*	2.71	0.018	Signal transduction	
101058_at	*Amy1*	5.59	0.019	Carbohydrate metabolism	
c.					
96742_at	*Dpt*	2.84	0.033	Cell adhesion	ECM
104445_at	*4631408011Rik*	2.63	0.002		
99671_at	*Adn*	6.51	0.008	Complement activation	Extracellular space
160375_at	*Car3*	7.18	0.044	One-carbon compound metabolism	
93353_at	*Lum*	2.11	0.022		ECM
93534_at	*Dcn*	2.44	0.013		ECM
d.					
99081_at	*Serping1*	1.79	0.041	Complement activation	Extracellular space
92833_at	*Hal*	2	0.049	Amino acid metabolism	
B. Genes up-regulated in tumors at malignant transition					
98627_at	*Igfbp2*	1.41	0.016	Cell growth regulation	Extracellular space
99952_at	*Chi3l1*	2.13	0.048	Carbohydrate metabolism	Extracellular space
161046_at	*Crlf1*	2.03	0.011	Antipathogenic response	
162206_f_at	*Socs3*	1.8	0.069†	Cell growth regulation	
162483_f_at	*Col18a1*	1.64	0.096†	Cell adhesion	ECM

*Fold change of averaged tumor signal value compared with averaged MIN-O signal value calculated in MAS 5.0.
†These probes were chosen based on the results from other data analysis (Supplemental data 2).

Sncg). In addition, we picked *Serping1*, a member of serine proteinase inhibitor family, because another member of serine proteinase inhibitor family, *Maspin*, is a well-studied tumor suppressor in human breast cancer (35, 36). The quantitative RT-PCR analysis of *Thrsp*, *Sncg*, and *Serping1* expression patterns correlated with the microarray analysis (Fig. 4, *columns 1* and *2*). These genes were consistently expressed at higher levels in MIN-Os than in tumors. The expression levels in prelactating fat pads also correlated well for all three genes, but we did find some discrepancies in the gene expression profiles in the virgin fat pads. This difference may be due to the fact that we used RNA from different virgin glands for the microarray and quantitative RT-PCR analysis.

We also used total RNA from other MIN-O and tumor samples from this line for quantitative RT-PCR analysis (Fig. 4, *column 3*). *Sncg* and *Serping1* expression values were higher in all three MIN-O samples compared with the tumors. *Thrsp*, on the other hand, in these MIN-O and tumor samples failed to show statistically significant expression differences. However, when the paired samples (5262 and 5263) were compared, *Thrsp* expression in the tumors was equivalent or lower than that in the MIN-O samples.

For two additional genes, IHC was used to verify and localize the protein products of differentially expressed genes. According to the expression analysis, *Igfbp2* exhibited increased expression in tumors, although it was scarcely expressed in the normal fat pads (Fig. 5A). Because the up-regulation of *Igfbp2* mRNA and protein in human breast cancer has been reported previously (24, 25), we investigated the Igfbp2 protein expression in the mammary fat pads (Fig. 5B). Antibody specific to Igfbp2 detected very low expression in normal mammary fat pads, mostly found secreted in the ducts. In the MIN-Os, patchy cytoplasmic expression was detected (Fig. 5B). In the center, away from the proliferative peripheral region, some myoepithelium-like staining was observed. However, this pattern did not overlap with smooth muscle actin expression (Fig. 5C); thus, it is unlikely that these Igfbp2-positive cells are myoepithelial. In the tumors, Igfbp2 was expressed at higher levels in a global cytoplasmic pattern with random patches of very strong positivity within the tumor.

Dcn was one of the genes down-regulated at the malignant transition. Dcn is a small proteoglycan of extracellular matrix (ECM) that is dysregulated in human breast carcinoma (32, 37). The transcript level of *Dcn* was down-regulated by >2-fold at

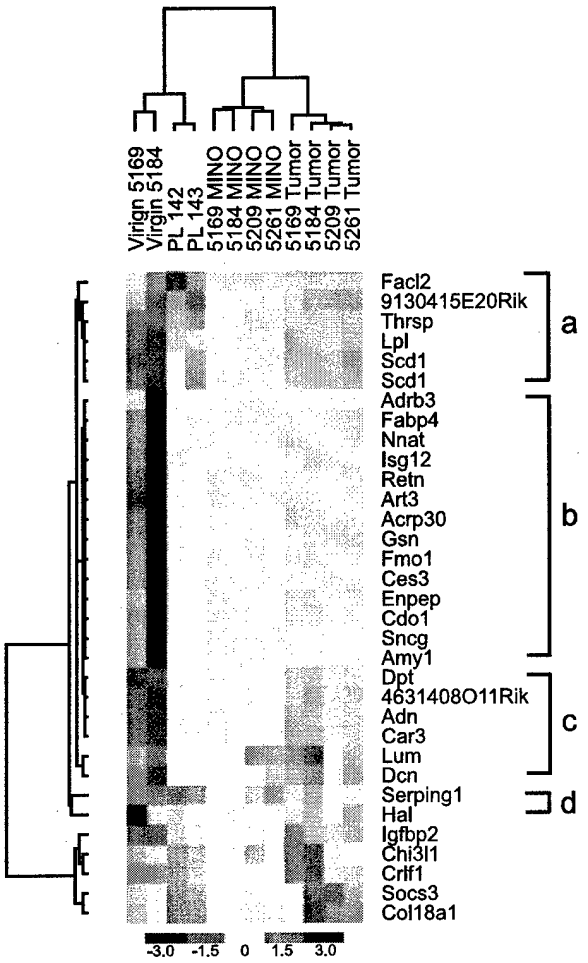

FIGURE 3. Hierarchical clustering of normal, MIN-O, and tumor samples using differentially expressed genes at the MIN-O/tumor transition. Down-regulated genes were further subgrouped based on the expression pattern in the normal samples (*a-d*).

the MIN-O/tumor transition, whereas the samples of normal tissue had even higher expression levels than the MIN-Os (Fig. 5D). According to the immunohistologic analysis, the Dcn protein is localized in stroma of the normal fat pad (Fig. 5G) as well as of the MIN-O (Fig. 5E). In the outgrowths, Dcn positivity was found in the stroma surrounding the microacinar clusters. In contrast, the stromal positivity was lost in the tumors, although they retained the microacinar architecture and had associated stroma (Fig. 5E and F). Dcn was expressed throughout the stroma of prelactating fat pads. Interestingly, in the prelactating fat pads, the strongest staining of Dcn was found to highlight septa within the stroma (Fig. 5G and H).

Discussion

Mouse mammary tumorigenesis has traditionally been divided into two major processes that involve the transition from normal to premalignant *in situ* (called nodulogenesis) and the transition from premalignant to malignant (called tumorigenesis; refs. 38-40). The GEM-based PyV-mT transplantation model described here has morphologic and biological transitions similar to other GEM mouse mammary tumor models (8). This model, however, is unique because it uses a transplantable premalignant tissue initiated by the expression of a specific molecule (PyV-mT).

Using a stringent difference requirement, we found a rather large number (132 genes) of transcriptome changes, most of which were gene inductions that occur during the premalignant transition from normal to the *in situ* PyV-mT MIN. In contrast, considerably fewer gene expression changes (32 genes), largely down-regulation, occur during the malignant transition from MIN-O to tumor. These findings suggest that major changes in the molecular architecture of the cell appear during the premalignant transformation, and activation of oncogenic transcription may be initiated at this stage. The transition to malignancy does not coincide with dramatic change in transcription but may be regulated by other post-transcriptional changes.

Many of the 132 differences identified during premalignant transformation were genes that have already been found to be associated with human breast and other cancers. These molecular differences are unlikely to reflect the differences in cell type composition between the normal fat pad and the MIN-O, because the differences were extrapolated by using two different types of "normal" mammary fat pads (adipose-enriched virgin fat pad and gland-enriched prelactating fat pad).

Despite the significant differences in their morphology and malignant behavior, very few transcript changes were associated with the MIN-O to tumor transition. Moreover, the MIN-O and tumor pairs segregated together in unbiased hierarchical clustering analysis (Fig. 2B). These results show that these biologically and morphologically disparate tissues can have remarkable molecular similarities. A similar trend was observed in human breast cancer in which few transcriptional changes were identified by DNA microarray and serial analysis of gene expression between DCIS and the corresponding breast carcinoma from the same patients (3, 4). In fact, our MIN-O/tumor clustering pattern is remarkably similar to the hierarchical clustering of the human DCIS/invasive ductal carcinoma pairs described previously (3). Our data imply that, in both human and GEM, the preinvasive lesions already possess most of the genetic events needed for progression to malignancy. Previous studies of mouse mammary outgrowths have failed to establish morphologic predictors of biological potential, leaving the investigator with test-by-transplantation as the only criteria (18, 41). Our analysis supports a hypothesis that gene expression profiling may be able to serve as a more robust prognostic tool for determining the biological properties of the *in situ* neoplasm.

Of the 32 genes identified as differentially expressed between the PyV-mT MIN/tumor comparisons, eight have been associated with human breast cancer (*Socs3*, *Igfbp2*, *Chi3l1*, *Lum*, *Dcn*, *Gsn*, *Thrsp*, and *Sncg*). Increased expression of *Socs3*, *Igfbp2*, *Thrsp*, and *Sncg* have been reported in human breast cancer (23-29), and increased serum levels of *Chi3l1* have been reported in breast cancer patients (30). *Lum* and *Dcn* are abundantly expressed in normal breast tissue, but their reduced expression is associated with more invasive and aggressive breast cancer (33). Except for *Gsn*, which has been reported to show down-regulation with the progression from normal to DCIS to invasive breast cancer (34, 42), we have yet to find any report of expression studies of the remaining genes correlating with the different stages of breast cancer progression.

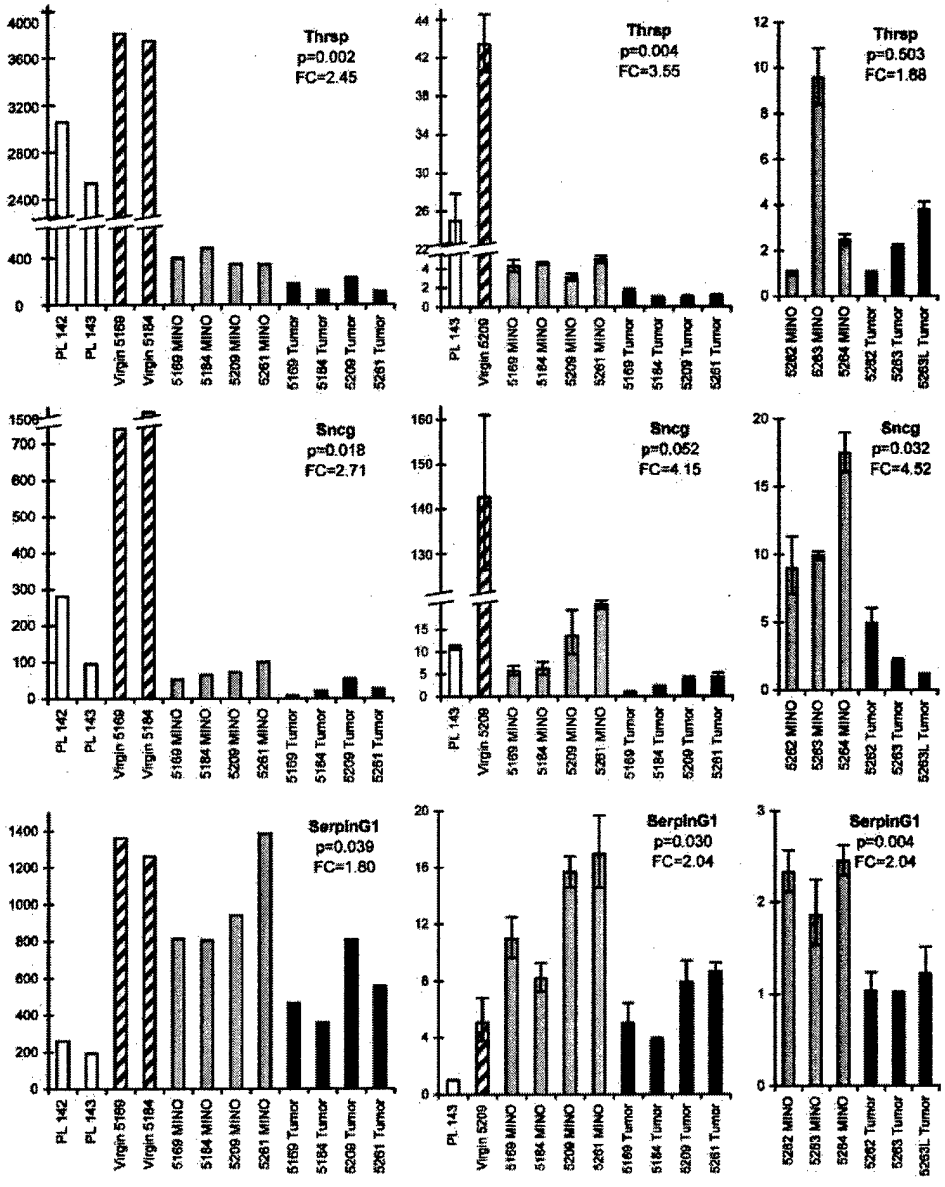

FIGURE 4. Expression levels of three identified genes: *Thrsp*, *Sncg*, and *Serping1*. Summary of microarray results (*left*) and relative expression analysis using semiquantitative real-time PCR (*center* and *right*). The samples used for microarray analysis, except for the normal RNA that was extracted from a different sample, were used for real-time PCR analysis (*center*). The real-time PCR analysis of different MIN-O and tumor samples from the 8w-B line (*right*).

The apparent dysregulation of insulin-related pathways has, to the best of our knowledge, not been previously documented in the PyV-mT tumors. *Igfbp2* expression is low in the normal mammary fat pad (average signal value of 147 in virgin and 16 in prelactating), whereas the expression increases as the tumor develops (average signal value of 410 in MIN-O and 874 in tumor). A commercial antibody was used to show that the protein was highly expressed in the MIN-O and tumor epithelia. The tumor cells had strikingly heavy cytoplasmic staining (Fig. 5).

Igfbp2 is one of the six insulin-like growth factor (IGF) binding protein (IGFBP) that have high affinity for IGFs and that play an important role in modulating the IGF system. Various studies document the importance of this system in mammary development and tumorigenesis (43-45). For example, overexpression of IGF-I in mammary gland leads to hyperplasia and a failure of postlactational apoptosis. In combination with loss of p53, up-regulation of IGF-I leads to mammary tumors with a short latency (46). The role of IGFBPs is complex. They function as both positive and negative regulators of the IGF system; furthermore, IGF-independent actions of IGFBPs have been reported (47, 48).

Increased expression of Igfbp2 has been associated with various tumors, and the positive correlation with the expression level and tumor grade has been reported (24). A recent study using human prostate specimens and cell lines identified dramatic overexpression of Igfbp2 that was associated with malignant transformation (49). Igfbp2 stimulates malignant prostate cells but not normal prostate cells (50). This suggests that normal and malignant epithelial cells have different susceptibility toward the Igfbp2 action, which may reflect the availability of interacting molecules in the extracellular space.

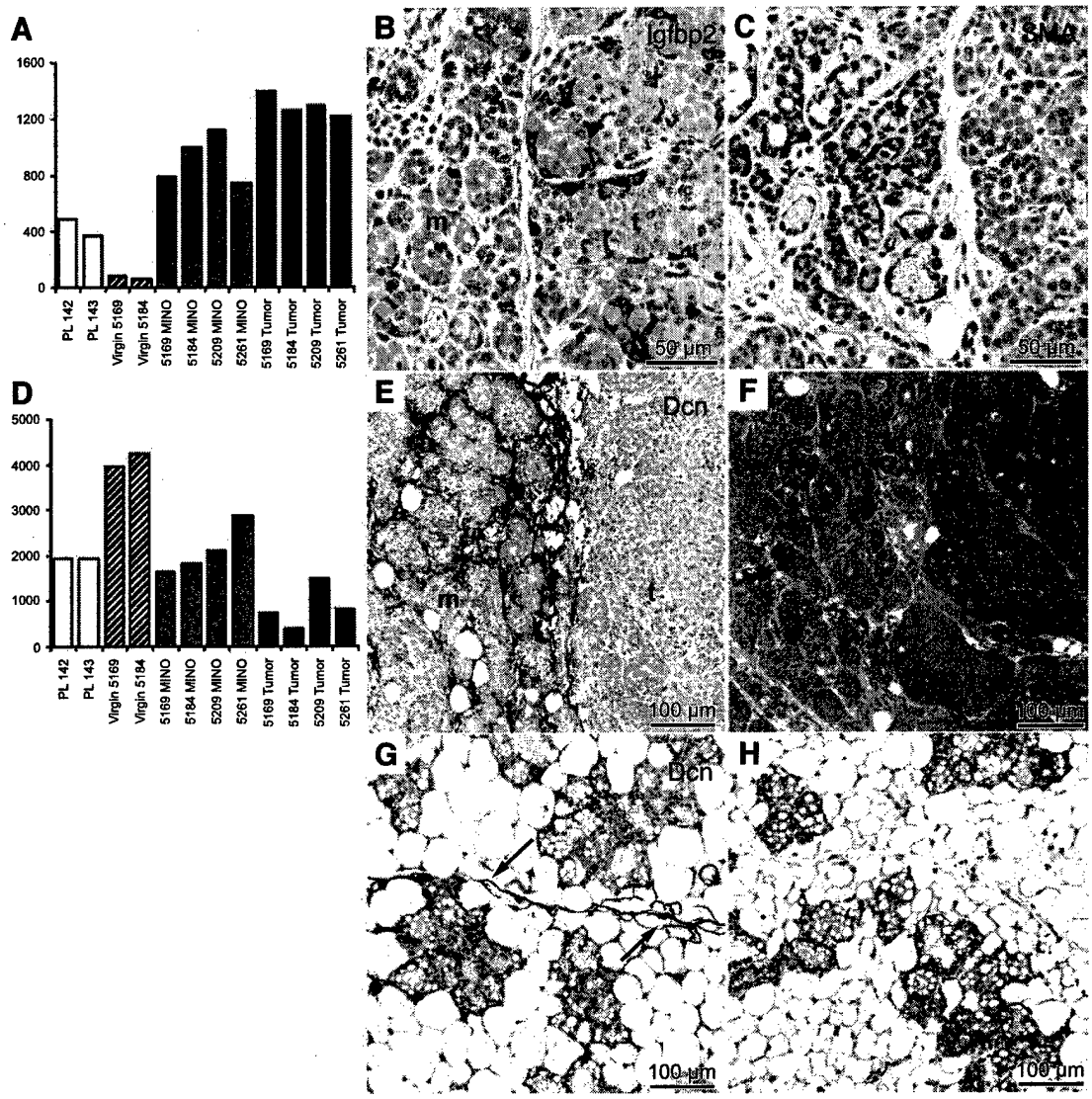

FIGURE 5. Expression levels of *Igfbp2* (**A**) and *Dcn* (**D**) from the microarray analysis. Igfbp2 (**B**) and smooth muscle actin (*SMA*; **C**) localization at the MIN-O (*m*)/tumor (*t*) interface on an 8w-B mammary fat pad. Igfbp2 is enriched in tumor compared with the adjacent MIN-O, and the Igfbp2-positive cells do not overlap with the smooth muscle actin–positive myoepithelium. IHC analysis of Dcn (**E** and **G**) and corresponding H&E (**F** and **H**) on an 8w-B (**E** and **F**) and a prelactating mammary fat pad (**G** and **H**). Dcn protein is readily detectable in the stroma of the MIN-O, whereas the staining is absent in the tumor. Weak Dcn expression is found throughout the stroma of prelactating fat pad (**G**), especially in major septi (*arrows*).

Another modulator of insulin signaling, *Socs3*, was up-regulated in our tumor samples. Increased expression of Socs3 is also found in human DCIS and invasive ductal carcinoma (23). In addition to its role in the insulin signaling, Socs3 acts to block the cytokine signal from the activated cytokine receptor and decrease cell sensitivity to other cytokines and hormones (51, 52). Interestingly, another cytokine-responsive protein, Crlf1, is also up-regulated in these GEM tumors. This may indicate the state of local host defense mechanism and implicates the stromal environment on tumor development.

Other components of the IGF system were differentially expressed at the normal/MIN-O transition. Although expressed in the MIN-Os and tumors, *IGF2* (which Igfbp2 preferential binds), *Igfbp3* (another IGFBP implicated in tumorigenesis), and *Igfbp4* were not expressed in virgin and prelactating mammary fat pads. The lack of expression in the normal mammary fat pad of these IGFBPs shows that they may be dysregulated early in the progression to invasive carcinoma. *Igfbp6*, on the other hand, was expressed in the proliferating fat pads and virgin mammary tissues but was not expressed in either the MIN-Os or the tumors. This observation is consistent with the observation that human breast cancer cells express Igfbp2, Igfbp3, Igfbp4, and Igfbp5.

Among the genes with reduced expression in tumors, we identified *Dcn*, an ECM-associated small leucine-rich proteoglycan. The expression of *Dcn* was down by >2-fold in tumors compared with the MIN-Os. The tumor stroma was essentially devoid of Dcn, whereas the normal stroma and the stroma of the

MIN-O were found to have abundant expression of Dcn. A similar observation has been made in human breast tissues in which *Dcn* mRNA and protein were expressed at lower levels in tumor-associated stroma compared with stroma associated with normal tissue (32). Previously, *in situ* hybridization analysis showed that *Dcn* is expressed by stromal cells of normal human breast tissue, DCIS, and invasive carcinoma; in particular, increased stromal expression rimming the DCIS was reported (37). More recently, low expression of Dcn and Lum, also identified in this study, was found to be associated with short progression time and poor prognosis in node-negative invasive breast cancer (33).

Several lines of experimental evidence suggest that Dcn directly interacts with transforming growth factor-β and epidermal growth factor receptor and that it has antiproliferative effects through the epidermal growth factor receptor and transforming growth factor-β pathways (53-55). Interestingly, our expression analysis identified another down-regulated ECM protein, Dpt, which directly interacts with Dcn and transforming growth factor-β (56). We suspect that these expression differences reflect the changes in the microenvironment and again highlight the contribution of stromal cells in tumor development.

In summary, our data support the hypothesis that the molecular changes occur very early in the progression to cancer and prior to the histopathologic identification of invasive cancer. The data presented here show that the transition from premalignancy to invasive carcinoma is associated with relatively few additional changes in gene expression. The genes related to the malignant transition in our GEM-derived model have also been identified as potential regulators of human breast cancer. These genes provide evidence for the dysregulation of the mitogenic signaling and the stromal-epithelial interaction as key regulators in the transition to invasive carcinoma.

We propose that this model closely mimics the development of invasive carcinoma in human breast. Together with other PyV-mT MIN-O lines, the 8w-B line provides an experimental system for understanding the biology of heterogeneous human DCIS lesions. These lines can be used to develop chemoprevention and therapeutic protocols for breast cancer in the future.

Material and Methods

Animals

The serial transplantation technique (57) and the establishment of the mouse PyV-mT MIN-O line 8w-B (9, 19) have been described previously. Serial transplantation of the premalignant MIN-O tissue bilaterally into the gland-cleared no. 4 mammary fat pads of recipient FVB virgin females (The Jackson Laboratory, Bar Harbor, ME) was carried out at 5-week intervals. MIN-Os and tumors were collected over four consecutive transplant generations (generations 9-12). In addition, intact nos. 2 and 3 mammary fat pads from the MIN-O transplant animals were collected and used as nontransgenic virgin mammary fat pads. Prelactating mammary fat pads were collected from the no. 4 mammary fat pads of 16-day pregnant FVB animals.

Tumors and MIN-O tissues were identified under a stereomicroscope, and grossly distinct regions were carefully biopsied for serial transplantation or sampling for further analysis. Because the MIN-O growth is confined to within the host mammary fat pad, the MIN-O grows as a flat sheet into the approximate shape of the fat pad. In contrast, tumors emerge from the central regions of the MIN-Os and grow as raised foci of dense tissue with defined borders. Because of this difference in the growth patterns, tumors can be distinguished grossly from surrounding MIN-O tissue. Dissected samples were frozen immediately in liquid nitrogen and stored at −80°C for future molecular analysis. The remaining fat pad from each tumor/MIN-O site was fixed in 4% formalin and embedded in paraffin, and sections (4 μm) were stained with Mayer's H&E. The biopsied site on the H&E-stained sections of the corresponding mammary fat pad were evaluated histologically to confirm the origin of the frozen sample before any samples were used for the molecular studies.

Immunohistochemistry

IHC was done on paraffin sections (4 μm) as described previously (15). The following primary antibodies were used with the Vectastain ABC Elite Kit (Vector Laboratories, Burlingame, CA): rabbit anti–estrogen receptor (1:600, LabVision, Fremont, CA), rabbit anti-PyV-mT (1:400, gift from Dr. G. Walter, University of California-San Diego, La Jolla, CA), rabbit anti-decorin (1:300, R&D Systems, Inc., Minneapolis, MN), rabbit anti-IGFBP2 (1:400, Santa Cruz Biotechnology, Santa Cruz, CA), and anti-Ki67 (1:2,400, Novocastra Laboratories, Newcastle upon Tyne, United Kingdom). Anti–smooth muscle actin (1:1,000, DAKO) was used in conjunction with the Animal Research Kit (DAKO) according to the manufacturer's instructions.

RNA Isolation

Frozen tissue (20-50 mg) was homogenized in TRIzol (Invitrogen, Carlsbad, CA), and total RNA was extracted according to the manufacturer's protocol followed by reextraction with phenol/chloroform/isoamyl alcohol (25:24:1) mixture, pH 4.3, (Fisher Scientific, Pittsburgh, PA). The isolated total RNA was purified further with the RNeasy RNA isolation kit (Qiagen, Inc., Valencia, CA). Quantity and quality of final total RNA were examined with RNA 6000 Nano LabChip using the Agilent 2100 Bioanalyzer (Agilent Technologies, Palo Alto, CA) as well as spectrophotometrically.

Oligonucleotide Array

Purified total RNA (10 μg) was used for cDNA synthesis followed by *in vitro* transcription to incorporate biotin labels and subsequent hybridization to Murine Genome Array GeneChip U74Av2 (MG_U74Av2, Affymetrix) according to the manufacturer's protocol. The U74Av2 array represents ~6,000 well-characterized sequences from the mouse Unigene database and an additional ~6,000 less well-characterized sequences from the expressed sequence tag clusters in the Unigene database.

Data Analysis

Processing of individual GeneChip image files was carried out using Affymetrix MAS 5.0. Probes (n = 5,119) that were present in all the MIN-O samples were used to calculate the correlation coefficients between different groups of mammary tissue.

The image files of the MIN-O, virgin, prelactating, and tumor samples were processed in DNA-Chip Analyzer version 1.2 (58). The MIN-O and normal (virgin and prelactating) groups were compared to identify probes with at least 2-fold expression difference, at the lower boundary of the 90% confidence interval, with $P \leq 0.05$. The same criteria, as well as a less stringent fold change requirement (1.2-fold), were used to compare the MIN-O and tumor image files.

On the MAS 5.0 processed image files, pair-wise comparison of each MIN-O and tumor pair was done to identify genes with at least 2-fold expression differences in three of four pairs or 1.2-fold differences in all four pairs. Moreover, using the Data Mining Tool (Affymetrix), the MIN-O expression data were compared with that of the tumor groups to identify probes with at least 1.2-fold expression differences with $P < 0.05$. Probes, with detection signal considered absent in all samples by the MAS 5.0 analysis, were removed from the data set, and the remaining probe set data were log transformed and subjected to the Significance Analysis of Microarrays (59) to select probes with differential expression of 1.2-fold. The final list of genes was generated from the significant differences from DNA-Chip Analyzer version 1.2 (1.2-fold, $P < 0.05$) using confirmation with at least one additional methodology (MAS 5.0, Data Mining Tool, and Significance Analysis of Microarrays; Supplemental data 2).[4]

Hierarchical clustering analysis was carried out in DNA-Chip Analyzer version 1.2 using probes that showed significant variation across the samples, as defined by having a coefficient of variation (SD/mean) of >0.3 and being present in at least 50% of samples (Fig. 2); a second cluster was developed using the 33 probes that were consistently differentially expressed between the MIN-Os and tumors (Fig. 3).

Semiquantitative RT-PCR for PyV-mT

For quantitation of the PyV-mT expression, DNase-treated total RNA (2 μg) was reverse transcribed using the RETROscript kit (Ambion, Austin, TX) primed with a 1:1 mixture of oligo(dT) and random decamers. The following primers were used to amplify a small region within the PyV-mT gene: 5′-CCAGCTACCAGTCGCCGCCT-3′ and 5′-GCTCTGAGAGCAGCTCTGTG-3′. As a normalization control, cyclophilin primers were designed: 5′-CGAGCTGTTTGCAGACAAAG-3′ and 5′-TTCTTGCTGGTCTTGCCATT-3′. One tenth of the reverse transcribed reaction was used for the subsequent real-time PCR reaction (20 μl) with 0.5 μmol/L primers and SYBR green DNA dye (QuantiTect SYBR Green PCR kit, Qiagen) in the LightCycler Instrument (Roche, Basel, Switzerland). The PCR cycles for both sets of primer pairs were as follows: 95°C for 15 minutes, 35 cycles of 94°C for 15 seconds, 60°C for 20 seconds, and 72°C for 20 seconds followed by melting curve analysis. Each reaction was run in duplicate and each sample was normalized by cyclophilin expression.

For validation of the identified gene expression differences, DNase-treated total RNA (1 μg) was reverse transcribed with random hexamers using Superscript II (Invitrogen) followed by RNaseH digestion. The gene expression differences were validated by real-time PCR on the ABI Prism 7700 (Applied Biosystems, Foster City, CA) with the Assays-on-Demand Gene Expression Assays (Applied Biosystems). The cDNA generated from total RNA (20 ng) was used for PCR reactions (25 μL), and each reaction was done in triplicate on a 96-well plate. Eukaryotic 18S RNA was used as the normalization control.

Acknowledgments

We thank Erik T. McGoldrick for transplantation and sample collection; Robert J. Munn for help with the imaging; Judith E. Walls and Veronica Bigornia (Transgenic Pathology Laboratory, University of California-Davis Center for Comparative Medicine) for the IHC; Dawn Milliken and Ryan Davis (Gene Expression Shared Resource, University of California-Davis Cancer Center; 1 P30 CA93373-01) for processing the microarrays; Chindo Hicks for help with the Significance Analysis of Microarrays; the members of the Gregg Laboratory for technical assistance; and Stephenie Liu for critical reading of this article.

References

1. Krishnamurthy S, Sneige N. Molecular and biologic markers of premalignant lesions of human breast. Adv Anat Pathol 2002;9:185–97.

2. Wellings SR, Jensen HM. On the origin and progression of ductal carcinoma in the human breast. J Natl Cancer Inst 1973;50:1111–8.

3. Ma XJ, Salunga R, Tuggle JT, et al. Gene expression profiles of human breast cancer progression. Proc Natl Acad Sci U S A 2003;100:5974–9.

4. Porter D, Lahti-Domenici J, Keshaviah A, et al. Molecular markers in ductal carcinoma *in situ* of the breast. Mol Cancer Res 2003;1:362–75.

5. Porter DA, Krop IE, Nasser S, et al. A SAGE (serial analysis of gene expression) view of breast tumor progression. Cancer Res 2001;61:5697–702.

6. Medina D. Biological and molecular characteristics of the premalignant mouse mammary gland. Biochim Biophys Acta 2002;1603:1–9.

7. Schulze-Garg C, Lohler J, Gocht A, Deppert W. A transgenic mouse model for the ductal carcinoma *in situ* (DCIS) of the mammary gland. Oncogene 2000; 19:1028–37.

8. Cardiff RD, Moghanaki D, Jensen RA. Genetically engineered mouse models of mammary intraepithelial neoplasia. J Mammary Gland Biol Neoplasia 2000; 5:421–37.

9. Maglione JE, Moghanaki D, Young LJ, et al. Transgenic polyoma middle-T mice model premalignant mammary disease. Cancer Res 2001;61:8298–305.

10. Guy CT, Cardiff RD, Muller WJ. Induction of mammary tumors by expression of polyomavirus middle T oncogene: a transgenic mouse model for metastatic disease. Mol Cell Biol 1992;12:954–61.

11. Wright C, Angus B, Nicholson S, et al. Expression of c-erbB-2 oncoprotein: a prognostic indicator in human breast cancer. Cancer Res 1989;49:2087–90.

12. Slamon DJ, Clark GM, Wong SG, Levin WJ, Ullrich A, McGuire WL. Human breast cancer: correlation of relapse and survival with amplification of the HER-2/neu oncogene. Science 1987;235:177–82.

13. Muller WJ, Ho J, Siegel PM. Oncogenic activation of Neu/ErbB-2 in a transgenic mouse model for breast cancer. Biochem Soc Symp 1998;63:149–57.

14. Barnes DM, Bartkova J, Camplejohn RS, Gullick WJ, Smith PJ, Millis RR. Overexpression of the c-erbB-2 oncoprotein: why does this occur more frequently in ductal carcinoma *in situ* than in invasive mammary carcinoma and is this of prognostic significance? Eur J Cancer 1992;28:644–8.

15. Rosner A, Miyoshi K, Landesman-Bollag E, et al. Pathway pathology: histological differences between ErbB/Ras and Wnt pathway transgenic mammary tumors. Am J Pathol 2002;161:1087–97.

16. Lin EY, Jones JG, Li P, et al. Progression to malignancy in the polyoma middle T oncoprotein mouse breast cancer model provides a reliable model for human diseases. Am J Pathol 2003;163:2113–26.

17. Desai KV, Xiao N, Wang W, et al. Initiating oncogenic event determines gene-expression patterns of human breast cancer models. Proc Natl Acad Sci U S A 2002;99:6967–72.

18. Cardiff RD, Anver MR, Gusterson BA, et al. The mammary pathology of genetically engineered mice: the consensus report and recommendations from the Annapolis meeting. Oncogene 2000;19:968–88.

19. Maglione JE, McGoldrick ET, Young LJT, et al. PyV-mT-induced MIN outgrowths: single origin, divergent evolution, multiple outcomes. Mol Cancer Ther. In press 2004.

20. Jerry DJ, Kittrell FS, Kuperwasser C, et al. A mammary-specific model

demonstrates the role of the p53 tumor suppressor gene in tumor development. Oncogene 2000;19:1052–8.

21. Medina D, Kittrell FS, Shepard A, et al. Biological and genetic properties of the p53 null preneoplastic mammary epithelium. FASEB J 2002;16:881–3.

22. Perou CM, Sorlie T, Eisen MB, et al. Molecular portraits of human breast tumors. Nature 2000;406:747–52.

23. Raccurt M, Tam SP, Lau P, et al. Suppressor of cytokine signaling gene expression is elevated in breast carcinoma. Br J Cancer 2003;89:524–32.

24. Pekonen F, Nyman T, Ilvesmaki V, Partanen S. Insulin-like growth factor binding proteins in human breast cancer tissue. Cancer Res 1992;52:5204–7.

25. McGuire SE, Hilsenbeck SG, Figueroa JA, Jackson JG, Yee D. Detection of insulin-like growth factor binding proteins (IGFBPs) by ligand blotting in breast cancer tissues. Cancer Lett 1994;77:25–32.

26. Cunningham BA, Moncur JT, Huntington JT, Kinlaw WB. "Spot 14" protein: a metabolic integrator in normal and neoplastic cells. Thyroid 1998;8:815–25.

27. Moncur JT, Park JP, Memoli VA, Mohandas TK, Kinlaw WB. The "Spot 14" gene resides on the telomeric end of the 11q13 amplicon and is expressed in lipogenic breast cancers: implications for control of tumor metabolism. Proc Natl Acad Sci U S A 1998;95:6989–94.

28. Ji H, Liu YE, Jia T, et al. Identification of a breast cancer-specific gene, BCSG1, by direct differential cDNA sequencing. Cancer Res 1997;57:759–64.

29. Bruening W, Giasson BI, Klein-Szanto AJ, Lee VM, Trojanowski JQ, Godwin AK. Synucleins are expressed in the majority of breast and ovarian carcinomas and in preneoplastic lesions of the ovary. Cancer 2000;88:2154–63.

30. Johansen JS, Cintin C, Jorgensen M, Kamby C, Price PA. Serum YKL-40: a new potential marker of prognosis and location of metastases of patients with recurrent breast cancer. Eur J Cancer 1995;31A:1437–42.

31. Leygue E, Snell L, Dotzlaw H, et al. Expression of lumican in human breast carcinoma. Cancer Res 1998;58:1348–52.

32. Leygue E, Snell L, Dotzlaw H, et al. Lumican and decorin are differentially expressed in human breast carcinoma. J Pathol 2000;192:313–20.

33. Troup S, Njue C, Kliewer EV, et al. Reduced expression of the small leucine-rich proteoglycans, lumican, and decorin is associated with poor outcome in node-negative invasive breast cancer. Clin Cancer Res 2003;9:207–14.

34. Asch HL, Winston JS, Edge SB, Stomper PC, Asch BB. Down-regulation of gelsolin expression in human breast ductal carcinoma *in situ* with and without invasion. Breast Cancer Res Treat 1999;55:179–88.

35. Maass N, Hojo T, Rosel F, Ikeda T, Jonat W, Nagasaki K. Down regulation of the tumor suppressor gene maspin in breast carcinoma is associated with a higher risk of distant metastasis. Clin Biochem 2001;34:303–7.

36. Maass N, Nagasaki K, Ziebart M, Mundhenke C, Jonat W. Expression and regulation of tumor suppressor gene maspin in breast cancer. Clin Breast Cancer 2002;3:281–7.

37. Brown LF, Guidi AJ, Schnitt SJ, et al. Vascular stroma formation in carcinoma *in situ,* invasive carcinoma, and metastatic carcinoma of the breast. Clin Cancer Res 1999;5:1041–56.

38. Cardiff RD, Wellings SR, Faulkin LJ. Biology of breast preneoplasia. Cancer 1977;39:2734–46.

39. Medina D. Preneoplastic lesions in mouse mammary tumorigenesis. In: Busch H, editor. Methods in cancer research. Vol. 7. New York: Academic Press; 1973. p. 3–53.

40. Faulkin LJ Jr, Deome KB. Regulation of growth and spacing of gland elements in the mammary fat pad of the C3H mouse. J Natl Cancer Inst 1960; 24:953–69.

41. Medina D. The preneoplastic phenotype in murine mammary tumorigenesis. J Mammary Gland Biol Neoplasia 2000;5:393–407.

42. Winston JS, Asch HL, Zhang PJ, Edge SB, Hyland A, Asch BB. Downregulation of gelsolin correlates with the progression to breast carcinoma. Breast Cancer Res Treat 2001;65:11–21.

43. Wood TL, Yee D. Introduction: IGFs and IGFBPs in the normal mammary gland and in breast cancer. J Mammary Gland Biol Neoplasia 2000;5:1–5.

44. Yee D. The insulin-like growth factor system as a treatment target in breast cancer. Semin Oncol 2002;29:86–95.

45. Furstenberger G, Senn HJ. Insulin-like growth factors and cancer. Lancet Oncol 2002;3:298–302.

46. Hadsell DL, Murphy KL, Bonnette SG, Reece N, Laucirica R, Rosen JM. Cooperative interaction between mutant p53 and des(1-3)IGF-I accelerates mammary tumorigenesis. Oncogene 2000;19:889–98.

47. Duan C. Specifying the cellular responses to IGF signals: roles of IGF-binding proteins. J Endocrinol 2002;175:41–54.

48. Mohan S, Baylink DJ. IGF-binding proteins are multifunctional and act via IGF-dependent and -independent mechanisms. J Endocrinol 2002;175:19–31.

49. Richardsen E, Ukkonen T, Bjornsen T, Mortensen E, Egevad L, Busch C. Overexpression of IGBFB2 is a marker for malignant transformation in prostate epithelium. Virchows Arch 2003;442:329–35.

50. Moore MG, Wetterau LA, Francis MJ, Peehl DM, Cohen P. Novel stimulatory role for insulin-like growth factor binding protein-2 in prostate cancer cells. Int J Cancer 2003;105:14–9.

51. Emanuelli B, Peraldi P, Filloux C, Sawka-Verhelle D, Hilton D, Van Obberghen E. SOCS-3 is an insulin-induced negative regulator of insulin signaling. J Biol Chem 2000;275:15985–91.

52. Larsen L, Ropke C. Suppressors of cytokine signaling: SOCS. APMIS 2002; 110:833–44.

53. Moscatello DK, Santra M, Mann DM, McQuillan DJ, Wong AJ, Iozzo RV. Decorin suppresses tumor cell growth by activating the epidermal growth factor receptor. J Clin Invest 1998;101:406–12.

54. Iozzo RV, Moscatello DK, McQuillan DJ, Eichstetter I. Decorin is a biological ligand for the epidermal growth factor receptor. J Biol Chem 1999; 274:4489–92.

55. Yamaguchi Y, Mann DM, Ruoslahti E. Negative regulation of transforming growth factor-β by the proteoglycan decorin. Nature 1990;346:281–4.

56. Okamoto O, Fujiwara S, Abe M, Sato Y. Dermatopontin interacts with transforming growth factor β and enhances its biological activity. Biochem J 1999;337 Pt 3:537–41.

57. Young LJT. The cleared mammary fat pad and the transplantation of mammary gland morphological structures and cells. In: Ipand MM, Asch BB, editors. Methods in mammary gland biology and breast cancer research. New York: Kluwer Academic/Plenum Publishers; 2000. p. 67–74.

58. Li C, Wong WH. Model-based analysis of oligonucleotide arrays: expression index computation and outlier detection. Proc Natl Acad Sci U S A 2001;98:31–6.

59. Tusher VG, Tibshirani R, Chu G. Significance analysis of microarrays applied to the ionizing radiation response. Proc Natl Acad Sci U S A 2001;98:5116–21.